

# The role of spatial correlations in same-material tribocharging

Galien Grosjean,\* Sebastian Wald, Juan Carlos Sobarzo, and Scott Waitukaitis  
*IST Austria*

*Lab Building West  
 Am Campus 1*

*3400 Klosterneuburg AT*  
 (Dated: May 18, 2022)

The observation of charge mosaics suggests that same-material tribocharging may arise via surface heterogeneity. However, the origin of this heterogeneity, as well as the role of spatial correlations within it, are unaddressed. Here we reveal how spatial correlations affect the surface heterogeneity mechanism. We find that correlations dramatically enhance the scale of charge transfer, while effectively suppressing fluctuations. Addressing origins, we show that a nucleation process that energetically favors neighboring donors is a viable candidate. Our work gives fundamental insight into the role of spatial correlations in the surface heterogeneity mechanism for same-material tribocharging.

Tribocharging, *i.e.* charge transfer between materials during contact [1], plays a critical role in natural phenomena [2–6], industrial processes [7, 8], and energy harvesting devices [9–11], but is not well-understood. One particularly perplexing issue is that even identical materials, when brought into contact, systematically transfer charge [12–21]. Several mechanisms could be involved in this ‘same-material’ tribocharging, including ones based on localized stresses [22], trapped electrons [23–27], induced polarization [28–32], or mechanochemistry [7, 33–35]. Alternatively, some experiments suggest that the required symmetry breaking could be more subtle, involving statistical fluctuations in the properties of the material itself [15, 16, 20, 36, 37]. Apodaca *et al.* found that the scale of same-material charge transfer grows with the square root of the contacting area [15], which led them to propose the existence of heterogeneity in the donor/acceptor nature of the surface. Partitioning the surfaces into equally sized donor/acceptor sites and assuming they are *uncorrelated*, one recovers  $|\Delta Q| = C\sqrt{A}$ , with the prefactor depending on the site density,  $N/A$ . Physically, one would expect about one donor/acceptor per atom at most, yet the value required to explain the data in Ref. [15] ( $2.90 \times 10^{18} \text{ mm}^{-2}$ ) corresponds to sites whose side lengths are approximately  $0.005 \text{ \AA}$ —more than 100 times smaller than the Bohr radius of hydrogen.

Nonetheless, features reminiscent of this model have been observed, but at significantly larger lengthscales. Using Kelvin Force Probe Microscopy, Baytekin *et al.* found neighboring regions of positive/negative charge with sizes from tens to hundreds of nanometers [16]. These charge ‘mosaics’ raise numerous questions. How can the unrealistically small lengthscales implied by Ref. [15] be rationalized with the much larger scales of mosaics? How would spatial correlations alter the surface heterogeneity model? And what physical process(es) create heterogeneity with spatial correlations in the first place? Here, we investigate how spatial correlations affect the surface heterogeneity model for same-material

tribocharging. Foremost, we find that correlations dramatically increase the scale of charge transfer in a single contact. For sequential contacts, we determine how correlations affect the average behavior, but also how

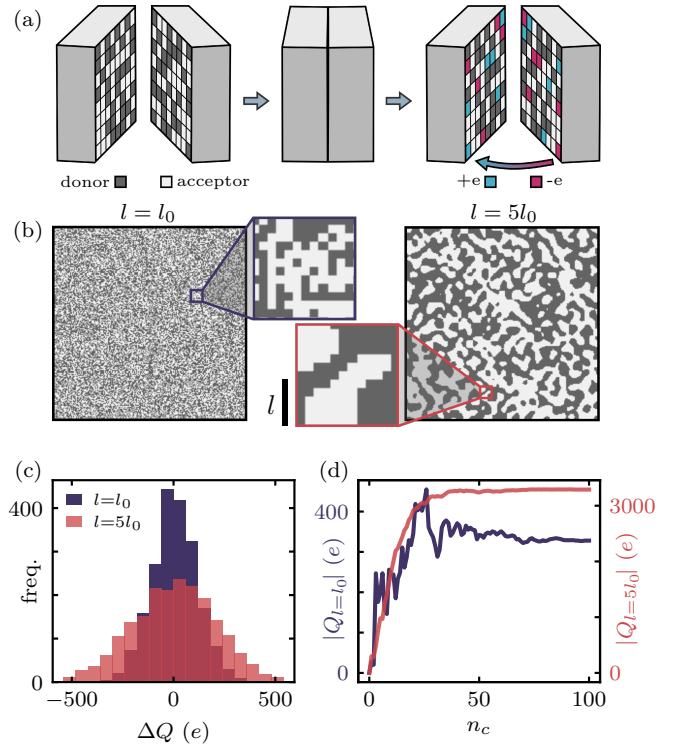


FIG. 1. (a) Same-material tribocharging may arise from surface heterogeneity [15], where donor/acceptor sites transfer unit charges,  $e$ , during contact. (b) Surfaces with identical donor probabilities  $p$ , but different correlation lengths,  $l$ ; on the left,  $l = l_0$ , and on the right  $l = 5l_0$  ( $l_0$  is the site size). (c) The single-contact distribution in  $\Delta Q$  is broader when  $l = 5l_0$  (violet,  $\sim 200 e$ ) than when  $l = l_0$  (pink,  $\sim 100 e$ ). (d) For sequential contacts, charge transfer is enhanced when  $l = 5l_0$ , and fluctuations that dominate the  $l = l_0$  case are suppressed.

they suppress fluctuations. Finally, we address the origin of the heterogeneity, revealing that a nucleation process where donor sites ‘prefer’ to be close is a viable candidate.

We simulate charge transfer between ‘synthetic’ surfaces (in contrast to physically derived surfaces later) by creating two  $N$ -element matrices involving three length-scales:  $l_0$ ,  $l$ , and  $L$ . The smallest,  $l_0$ , corresponds to an elementary donor/acceptor and is represented by a single matrix element. The largest,  $L$ , corresponds to the system size. We assume that there is a single intermediate scale,  $l$ , that characterizes correlations. Each matrix element is assigned as donor or acceptor, with probabilities  $p$  and  $1 - p$ , respectively. We account for correlations in assignments via thresholding a random scalar field (see Supplemental Material [38]). During ‘contact’, we generate a ‘left’ and ‘right’ surface from identical input length-scales and probabilities. Charge transfer of one unit,  $e$ , between matrix elements  $[i, j]$  occurs if (1)  $[i, j]$  on the left/right is a donor, (2)  $[i, j]$  on the right/left is an acceptor, (3) the value of an independent random uniform variable is less than the transfer probability,  $\alpha$ , and (4) for sequential contacts, transfer at  $[i, j]$  hasn’t yet occurred. The net charge transferred is the difference between left-to-right (‘right’) and right-to-left (‘left’) transfers.

Figure 1 shows two representative surfaces, one with  $l = l_0$  and the second  $l = 5 l_0$  ( $p = 0.5$ ). Although their only difference involves spatial correlations, we see stark changes in the charging behavior. In Fig. 1c, we plot distributions of the charge transferred in the first contact,  $\Delta Q$ , for 1000 pair-instances. Both are Gaussian and centered at zero, but while  $l = l_0$  produces a width of  $\sim 100 e$ , the  $l = 5 l_0$  width is  $\sim 200 e$ . Correlations also change the behavior during sequential contacts. Fig. 1d shows two examples of the accumulated charge,  $|Q|$ , vs. the number of contacts,  $n_c$ . Like the initial transfer, the final charge,  $Q_f$ , is typically larger when  $l = 5 l_0$ . Additionally, the fluctuations are on the order of  $Q_f$  when  $l = l_0$ , but are hardly discernible when the  $l = 5 l_0$  (consistent with experiments [15]).

In Fig. 2, we examine the first contact behavior in detail. Fig. 2a shows the average absolute value of charge exchanged,  $|\overline{\Delta Q}|$ , for increasing system size and several values of  $l$ . The scaling  $|\overline{\Delta Q}| \propto \sqrt{A} \propto L/l_0$  is recovered in all cases, but the prefactor steadily increases with  $l > l_0$ . Fig. 2b shows that the dependence on the transfer probability,  $\alpha$ , exhibits unexpected non-linear behavior. At every value of  $l$ , we see a trend consistent with a power law, *i.e.*  $|\overline{\Delta Q}| \propto \alpha^k$ . However, the exponent,  $k$ , increases with  $l$ , starting at  $k = 0.5$  for  $l = l_0$  and saturating at  $k = 1.0$  for  $l \gg l_0$  (Fig. 2d).

To explain these observations, we first consider the case  $L \gg l = l_0$ , here sketching our argument (details are in the Supplemental Material [38]). We momentarily focus on right transfers, which occur with compound probability  $p(1 - p)\alpha$ . Absent correlations,

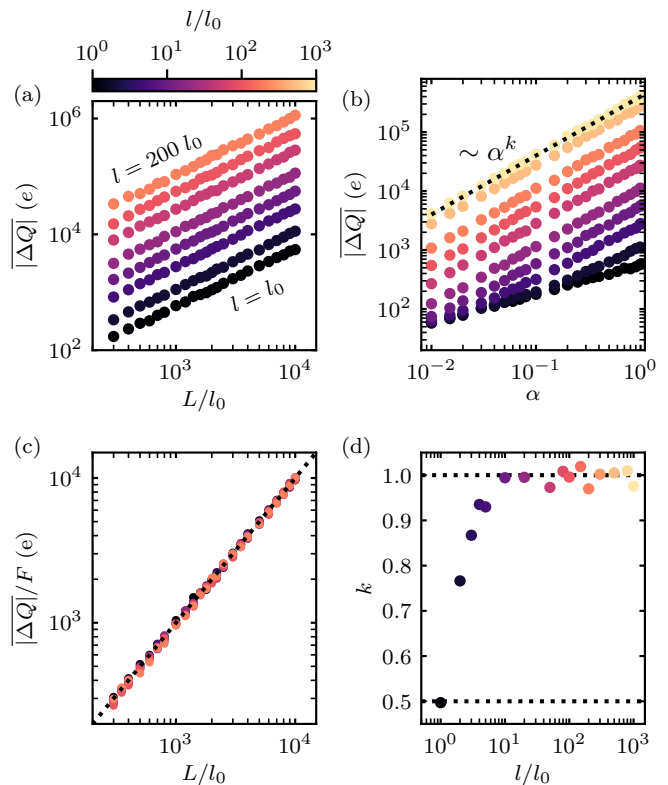


FIG. 2. (a) Average charge transfer  $|\overline{\Delta Q}|$  after one contact, for different values of  $l$  and  $L$  ( $\alpha = 1$ ,  $p = 0.5$ ). The scaling  $|\overline{\Delta Q}| \propto L$  is recovered in all cases, but with a growing prefactor. (b) For fixed  $L$  and  $l$ ,  $|\overline{\Delta Q}| \propto \alpha^k$ , where  $k$  changes with  $l$ . (c) The data from (a) for  $l \gg l_0$  collapses to a line of slope unity when rescaled using Eq. 2. (d) The exponent  $k$  vs.  $l/l_0$ . When  $l \approx l_0$ , transfer is probabilistic (Eq. 1) and  $|\overline{\Delta Q}| \propto \sqrt{\alpha}$ . When  $l \gg l_0$ , transfer occurs at a fixed rate (Eq. 2) where  $|\overline{\Delta Q}| \propto \alpha$ .

all sites  $[i, j]$  are independent, hence the total right charge transfer is Gaussian with mean  $eNp(1 - p)\alpha$  and width  $e\sqrt{Np(1 - p)\alpha(1 - p(1 - p)\alpha)}$ . A similar distribution exists for left transfer, but *only* when considered independently—simultaneous left/right transfer cannot occur. Nonetheless, this would have probability  $(p(1 - p)\alpha)^2$ , which is small. We therefore approximate the left/right distributions as independent. The net transfer,  $\Delta Q$ , is thus also Gaussian distributed, with zero mean and width  $\sigma = e\sqrt{2Np(1 - p)\alpha(1 - p(1 - p)\alpha)}$ . Neglecting terms like  $(p(1 - p)\alpha)^2$  and considering  $|\overline{\Delta Q}| = \sqrt{2/\pi}\sigma$  [38], we find

$$|\overline{\Delta Q}| = \sqrt{\frac{2}{\pi}} \frac{eL}{l_0} \sqrt{2p(1 - p)\alpha}. \quad (1)$$

This recovers the  $\sqrt{A}$  scaling, but differs from previous work [15] in that the  $\alpha$  dependence is square root rather than linear—exactly as we see in Fig. 1d. Physically, this must be the case: at the level of elementary parti-

cles, transfer is *intrinsically* probabilistic. In the Supplemental Material [38], we verify that Eq. 1 collapses our simulated data for wide ranges of  $p$  and  $\alpha$ .

Next we consider the case  $L \gg l \gg l_0$  (again with details in the Supplemental Material [38]). This fundamentally alters the argument above as the site identities exhibit spatial correlations. To account for this, we split the problem into two parts. First, we deal with the correlated donor/acceptor probabilities by rescaling the system by  $l/l_0$ , leading to surfaces with  $N' = N/(l/l_0)^2$  larger ‘sites’ or ‘patches’. We make the ansatz that identities of entire patches still occur with probabilities  $p$  and  $1 - p$ . Next, we rescale back to the original system to deal with transfers, which still occur independently for each site. During contact, regions of donors face acceptors with the characteristic size of a patch. If the number of sites in these regions ( $n = (l/l_0)^2$ ) is large, the mean transfer ( $\alpha n$ ) effectively hides the fluctuations ( $\sqrt{n\alpha(1-\alpha)}$ )—hence we treat  $\alpha$  as a rate. Thus, when  $l \gg l_0$  we have

$$|\overline{\Delta Q}| = \sqrt{\frac{2}{\pi}} \frac{e\alpha Ll}{l_0^2} \sqrt{2p(1-p)}. \quad (2)$$

Here, the dependence on  $\alpha$  is linear rather than square root (explaining the  $l \gg l_0$  limit in Fig. 2d). Additionally, the scale of transfer increases with  $l/l_0$ . In Fig. 2c, we confirm that rescaling the data from Fig. 2a by the prefactor  $F = \alpha l/l_0 \sqrt{4p(1-p)}/\pi$  collapses  $|\overline{\Delta Q}|$  when  $l \gg l_0$ . Ultimately, the increased charging arises because the variability in the number of donors/acceptors depends strongly on the scale of spatial correlations. This can be quickly grasped by considering the extreme case  $l=L$ , where each surface is either purely donor or acceptor, and consequently  $|\overline{\Delta Q}| \propto \alpha e N \propto A$ . This highlights that, in the surface-heterogeneity framework, same- and different-material tribocharging are two manifestations of a similar phenomenon, only appearing different depending on the scale at which one looks.

We now turn to sequential contacts. As shown in Fig. 3a, repeated contacts with the same surfaces leads to curves in accumulated charge,  $|Q|$  vs.  $n_c$ , that level off at some value,  $Q_f$ . In the Supplemental Material, we show that the underlying trend is given by a saturated exponential, *i.e.*,

$$Q(n_c) = Q_f (1 - \exp(-\alpha n_c)). \quad (3)$$

What is more interesting are the fluctuations on approach to  $Q_f$ . For large  $l/l_0$ , these aren’t noticeable, but for small  $l/l_0$  they are overwhelming. We quantify their scale by repeatedly performing first contacts between individual surface pairs (‘resetting’ each time) and measuring the fluctuations,  $\delta Q$  (Fig. 3b). In Fig. 3c we show  $\delta Q$  for a few pairs, which reveals that the fluctuations grow with  $L$  and depend strongly on  $\alpha$ , but are independent of  $l$ . To understand why, we note that a particular pair has a fixed donor/acceptor arrangement, which means

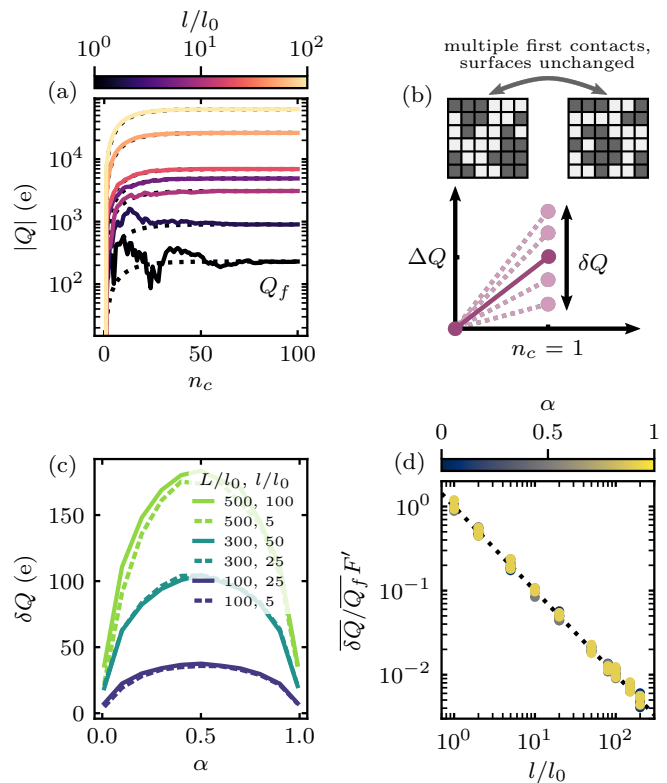


FIG. 3. (a) Sequential contacts lead to accumulated charge,  $|Q|$ , which ultimately saturates at  $Q_f$  (here for several  $l/l_0$ ,  $\alpha = 0.1$  and  $p = 0.5$ ). For small  $l/l_0$ , fluctuations are on the order of  $Q_f$ , whereas for large  $l$  they are suppressed. Dotted lines correspond to Eq. 3 using the measured  $Q_f$ . (b) We quantify fluctuations by repeating the first contact between the same two surfaces and measuring the spread,  $\delta Q$ . (c) For a particular surface pair,  $\delta Q$  depends on both  $\alpha$  and  $L$ , but is largely independent of  $l$ . (d) Ensemble averages of relative fluctuations  $\overline{\delta Q}/Q_f F'$  collapsed by factor  $F' = \sqrt{\alpha(1-\alpha)\pi}/2$  vs.  $l/l_0$ , which shows fluctuations are suppressed by spatial correlations. Each point corresponds to the ensemble average over 20 pairs of surfaces of the fluctuations over 50 contacts.

$\delta Q$  arises solely from  $\alpha$ . Denoting the number of donors on the left/right that face acceptors on the right/left as  $N_{\pm}$ , one finds that  $\delta Q = e\sqrt{(N_{\leftarrow} + N_{\rightarrow})\alpha(1-\alpha)}$ . In the Supplemental Material [38], we justify using the averages  $\overline{N_{\pm}} = (L/l_0)^2 p(1-p)$  to find the ensemble expression,

$$\overline{\delta Q} = e \frac{L}{l_0} \sqrt{2p(1-p)\alpha(1-\alpha)}. \quad (4)$$

This establishes that the fluctuations, like  $|\overline{\Delta Q}|$ , grow linearly with  $L$ , but unlike  $|\overline{\Delta Q}|$  are independent of  $l$ . Consequently, they cannot be suppressed by increasing system size, but can be suppressed by spatial correlations. In Fig. 3d, we collapse the  $\overline{\delta Q}$  simulation data to a predicted line with the appropriate rescaling.

Surface heterogeneity inherently features nontrivial spatial correlations, which we have shown significantly alter charge transfer. Still, the most fundamental ques-

tion remains unaddressed: what is the origin of the surface heterogeneity? We propose a nucleation process that energetically favors neighboring donors is a viable candidate. We support this by developing time-dependent, latticed-based simulations that physically mimic surface formation, again yielding  $L/l_0 \times L/l_0$  donor/acceptor matrices. At each time step, a donor site can transition into an acceptor site, and vice-versa. The transition probabilities depend on the neighboring sites, *i.e.*,

$$\begin{aligned} P_A(\nu) &= P_0 \exp(-K\nu) \\ P_D(\nu) &= P_0 \exp(-K(4-\nu)), \end{aligned} \quad (5)$$

where  $\nu$  is the number of neighbors that are donors (*i.e.*  $\nu \in [0, 4]$ ). The exponential form is motivated from an Arrhenius-like process where each neighbor modifies a local energy barrier by  $\epsilon/kT = K$ . We choose this form to distill simple ingredients that cause surface structures to emerge. Full details can be found in the Supplemental Material [38].

Starting with an initial arrangement, a surface evolves until it reaches a dynamic equilibrium set by the parameters in Eq. 5. Three examples for different  $K$  are shown in Fig. 4a (for a movie of the evolution, see the Supplemental Material [38]). To characterize these surfaces in the context of our analysis, we measure  $p$  and  $l/l_0$ . Determining  $p$  is trivial. To determine  $l/l_0$  we start by calculating the correlation function,

$$C(r) = \langle s(R)s(R+r) \rangle - \langle s(R) \rangle \langle s(R+r) \rangle, \quad (6)$$

where  $s$  is the site identity at a position  $R$ ,  $r$  is the distance from the point  $R$ , and averages denoted by  $\langle \rangle$  are over all sites separated by  $r$ . Figure 4b shows an example of  $C(r)$  for a particular surface. We use the first zero crossing to define the correlation length,  $l$ , as it corresponds to the typical distance before having an equal probability of switching from donor to acceptor (or *vice versa*). In the Supplemental Material, we show that this identically recovers the known correlation lengths in our synthetic surfaces [38]. In Figure 4c, we show how sweeping through the parameter  $K$  (keeping  $P_0$  fixed) allows us to explore approximately two orders of magnitude in  $l/l_0$  (with a stable donor probability  $p \approx 0.5$ ).

We use these simulated surfaces as input for contact experiments, with the rules for charge transfer the same as before. We generate 20 surfaces for various combinations of correlation length  $l/l_0$  and surface size  $L/l_0$ , and calculate  $|\Delta Q|$  for every permutation (Fig. 4d). The effect of spatial correlations in this physically-derived system is the same as with the synthetic surfaces, *i.e.* the scale of transfer increases with the correlation length. Figure 4e presents the results rescaled using Eq. 2, which largely collapses them onto a single line with the predicted unity slope. In the Supplemental Material [38], we explain how the slight deviation for intermediate values of  $K$  is due to the existence of a spectrum of length-scales in our physically-derived surfaces. Our definition

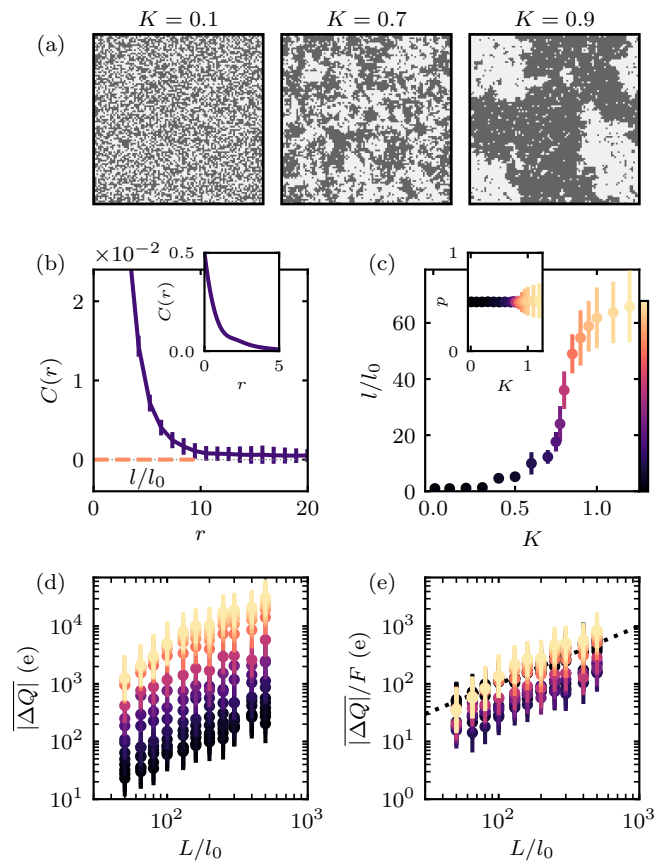


FIG. 4. (a) A generic nucleation process can lead to patches with a given size  $l > l_0$ . (b) We measure  $l/l_0$  using the radial correlation function (Eq. 6). We keep the same color scale for  $l/l_0$  in all subfigures. (c) We vary  $l/l_0$  through parameter  $K$  in Eq. 5. The inset shows that  $p$  remains constant. (d) As before, the charge transferred after a contact is drastically increased by the introduction of a lengthscale. (e) We verify that Eq. 2 is still valid. The dotted line is the identity line. Deviations at intermediate  $K$  are due to the presence of a spectrum of length-scales (see Supplemental Material [38]).

of the correlation length is sensitive to the largest correlated features, which renders the deviation small (factor of  $\sim 2$ ) owing to the fact that transfer is also dominated by the largest features since  $|\Delta Q| \propto l$  (see Supplemental Material [38]).

Our work stems from three well-supported assumptions: first, that charge transfer between insulators occurs locally [15, 20, 26, 27, 36, 37]; second, that single carriers transfer probabilistically [39, 40]; and third, same-material tribocharging involves surface heterogeneity [15, 16]. We have shown that spatial correlations play a crucial role. In a single contact, they affect the amount of charge transferred, leading to linear growth when  $l \gg l_0$ . In sequential contacts, they suppress fluctuations, leading to the smooth  $Q$  vs.  $n_c$  curves that are observed experimentally. Our results allow us to quantitatively resolve the inconsistency mentioned in the in-

roduction. Fitting the data from [15] with our form in Eq. 2 and using the larger lengthscale ( $l \approx 450$  nm) measured by [16], we extract a single site size of  $l_0 \approx 4$  Å, which corresponds to one donor/acceptor on an area the size of several atoms (see Supplemental Material [38]). This highlights the importance of spatial resolution in charge transfer simulations—for quantitative agreement, the correlation length must be resolved. Finally, we have addressed the origin of the surface heterogeneity, showing that a nucleation mechanism that energetically favors neighboring donors is sufficient. Our model is generic enough to be consistent with mechanisms such as adsorption of donors/acceptors (*e.g.* H<sub>2</sub>O) from the environment, but illustrates that neighboring sites cannot be treated as independent [20, 36, 41].

This project has received funding from the European Unions Horizon 2020 research and innovation programme under the Marie Skłodowska-Curie Grant Agreement No. 754411.

---

\* galienmariep.grosjean@ist.ac.at

- [1] D.J. Lacks and T. Shinbrot, *Nat. Rev. Chem.* **3**, 465-476 (2019).
- [2] T. Steinpilz, K. Joeris, F. Jungmann, D. Wolf, L. Brendel, J. Teiser, T. Shinbrot and G. Wurm, *Nat. Phys.* **16**, 225-229 (2020).
- [3] S.J. Desch and J.N. Cuzzi, *Icarus* **143**, 87-105 (2000).
- [4] G. Wurm, L. Schmidt, T. Steinpilz, L. Boden and J. Teiser, *Icarus* **331**, 103-109 (2019).
- [5] D.L. Schrader, K. Nagashima, S.R. Waitukaitis, J. Davidson, T.J. McCoy, H.C. Connolly Jr., and D.S. Lauretta, *Geochim. Cosmochim. Ac.* **223**, 405-421 (2018).
- [6] P. Berdeklis and R. List, *J. Am. Met. So.* **58**, 2751-2770 (2001).
- [7] H.T. Baytekin, B. Baytekin, T.M. Hermans, B. Kowalczyk and B.A. Grzybowski, *Science* **341**, 1368-1371 (2013).
- [8] T. Abbasi and S.A. Abbasi, *J. Hazard. Mat.* **140** 7-44 (2007).
- [9] M. Kanik, O. Aktas, H.S. Sen, E. Durgun and M. Bayindir, *ACS Nano* **8**, 9311-9323 (2014).
- [10] U.G. Musa, S.D. Cezan, B. Baytekin and H.T. Baytekin, *Sci. Rep.* **8**, 2472 (2018).
- [11] Z.L. Wang, *ACS Nano* **7** 9533-9557 (2013).
- [12] P.E. Shaw, *Nature* **118**, 659-660 (1926).
- [13] J. Lowell and W.S. Truscott, *J. Phys. D: Appl. Phys.* **19**, 1273-1280 (1986).
- [14] K.M. Forward, D.J. Lacks and R.M. Sankaran, *Geophys. Res. Lett.* **36**, L13201 (2009).
- [15] M.M. Apodaca, P.J. Wesson, K.J.M. Bishop, M.A. Ratner and B.A. Grzybowski, *Angew. Chem. Int. Ed.* **49**, 946-949 (2009).
- [16] H. T. Baytekin, A. Z. Patashinski, M. Branicki, B. Baytekin, S. Soh and B. A. Grzybowski, *Science* **333**, 308-312 (2011).
- [17] W. Hu, L. Xie and X. Zheng, *Appl. Phys. Lett.* **101**, 114107 (2012).
- [18] S.R. Waitukaitis and H.M. Jaeger, *Rev. Sci. Instrum.* **84**, 025104 (2013).
- [19] S.R. Waitukaitis, V. Lee, J.M. Pierson, S.L. Forman and H.M. Jaeger, *Phys. Rev. Lett.* **112**, 218001 (2014).
- [20] L. Xie, N. Bao, Y. Jiang and J. Zhou, *AIP Adv.* **6**, 035117 (2016).
- [21] V. Lee, N.M. James, S.R. Waitukaitis and H.M. Jaeger, *Phys. Rev. Mat.* **2**, 035602 (2018).
- [22] P. E. Shaw, *Proc. Phys. Soc.* **39**, 449 (1926).
- [23] J. Lowell and W. S. Truscott, *J. Phys. D: Appl. Phys.* **19**, 1281 (1986).
- [24] D. J. Lacks, N. Duff and S. K. Kumar, *Phys. Rev. Lett.* **100**, 188305 (2008).
- [25] D. J. Lacks and A. Levandovsky, *J. Electrostat.* **65**, 107-112 (2007).
- [26] N. Duff and D.J. Lacks, *J. Electrostat.* **66**, 51-57 (2008).
- [27] D.J. Lacks and R.M. Sankaran, *Particul. Sci. Technol.* **34**, 55-62 (2016).
- [28] T. Shinbrot, M. Rutala and H. Herrmann, *Phys. Rev. E* **96**, 032912 (2017).
- [29] T. Siu, J. Cotton, G. Mattson and T. Shinbrot, *Phys. Rev. E* **89**, 052208 (2014).
- [30] J. Kolehmainen, A. Ozel, Y. Gu, T. Shinbrot and S. Sundaresan, *Phys. Rev. Lett.* **121**, 124503 (2018).
- [31] R. Yoshimatsu, N.A.M. Araújo, G. Wurm, H.J. Herrmann and T. Shinbrot, *Sci. Rep.* **7**, 39996 (2016).
- [32] R. Yoshimatsu, N.A.M. Araújo, T. Shinbrot and H.J. Herrmann, *Soft Mat.* **12**, 62616267 (2016).
- [33] M. Sow, D.J. Lacks and M.R. Sankaran, *J. Appl. Phys.* **112**, 084909 (2012).
- [34] M. Sow, R. Widenor, A. Kumar, S.W. Lee, D.J. Lacks and R.M. Sankaran, *Angew. Chem. Int. Ed.* **51**, 2695 (2012).
- [35] M. Sow, D.J. Lacks and R.M. Sankaran, *J. Electrostat.* **71**, 396399 (2013).
- [36] I.A. Harris, M.X. Lim and H.M. Jaeger, *Phys. Rev. Mat.* **3**, 085603 (2019).
- [37] H. Yu, L. Mu and L. Xie, *J. Electrostat.* **90**, 113-122 (2017).
- [38] See Supplemental Material at [URL will be inserted by publisher] for additional details.
- [39] D.J. Lacks and M.R. Sankaran, *J. Phys. D: Appl. Phys.* **44**, 453001 (2011).
- [40] J.F. Kok and D.J. Lacks, *Phys. Rev. E* **79**, 051304 (2009).
- [41] M.D. Hogue, E.R. Mucciolo, C.I. Calle and C.R. Buhler, *J. Electrostat.* **63**, 179-188 (2005).